

Document downloaded from:

<http://hdl.handle.net/10251/77667>

This paper must be cited as:

Ortiz Serna, MP.; Sanchis Sánchez, MJ.; Redondo Foj, MB.; Carsí Rosique, M.; Díaz Calleja, R.; Leiva, A.; Gargallo, L.... (2015). Study of the dielectric relaxation of poly(phenylpropyl acrylate) and poly(phenylpropyl methacrylate): effect of slight differences in chemical structure. *Polymer International*. 64(12):1733-1740. doi:10.1002/pi.4973.



The final publication is available at

<http://dx.doi.org/10.1002/pi.4973>

Copyright Wiley

Additional Information

# Study of the dielectric relaxation of Poly(phenyl-propyl-acrylate) and Poly(phenyl-propyl-methacrylate): Effect of slight differences in the chemical structure

Pilar Ortiz-Serna<sup>a</sup>, Maria J. Sanchis<sup>a\*</sup>, Belén Redondo-Foj<sup>a</sup>, Marta Carsí<sup>b</sup>, Ricardo Díaz Calleja<sup>a</sup>, Angel Leiva<sup>c</sup>, Ligia Gargallo<sup>d</sup>, Deodato Radić<sup>c</sup>

## Abstract

A comparative study of the dielectric relaxational behavior of two structurally close polymers, containing aromatic side groups, was carried out in order to analyze how slight differences in the chemical structure affect the molecular responses to perturbation field. Specifically, poly-(phenyl-propyl-acrylate) (P3Ph1PA) and poly-(phenyl-propyl-methacrylate) (P3Ph1PM) were studied by Differential Scanning Calorimetry (DSC) and by Dielectric Relaxation Spectroscopy (DRS) in the frequency range of  $10^{-2}$ - $10^6$  Hz and temperature window of -80 to 120 °C. Both techniques showed one glass-rubber transition ( $T_g$ ) for the P3Ph1PA and two for the P3Ph1PM samples, which evidences the great effect of the methyl groups on the segmental motions of the polymer. Phenomenological analysis of the data has been carried out in order to establish the strength, width, and fragility parameters of the glass-rubber transitions. In the case of the P3Ph1PA, the strength was found to be larger than for the P3Ph1PM, pointing out that the methyl group disturbs the mobility. Conductive processes dominate the dielectric spectra at high temperatures and low frequencies.

**Keywords:** Differential Scanning Calorimetry, Dielectric Relaxation Spectroscopy, relaxational behavior, Poly-methacrylate, Poly-acrylate

\*Correspondence to: M. J. Sanchis, Departamento de Termodinámica Aplicada, Instituto de Tecnología Eléctrica, Universitat Politècnica de Valencia, Camino de Vera s/n, 46022 Valencia, Spain. E-mail: [jsanchis@ter.upv.es](mailto:jsanchis@ter.upv.es)

<sup>a</sup>Instituto Tecnología Eléctrica, Departamento de Termodinámica Aplicada, Universitat Politècnica de València, Camí de Vera s/n, 46022, Valencia, Spain

*<sup>b</sup>Instituto de Automática e Informática Industrial, Universitat Politècnica de València, Camí de Vera s/n, 46022, Valencia, Spain*

*<sup>c</sup>Departamento de Química Física, Pontificia Universidad Católica de Chile, Santiago, Chile*

*<sup>d</sup>Departamento de Química Facultad de Ciencias Universidad de Tarapacá Avda. General Velásquez 1775, Arica, Chile.*

## **INTRODUCTION**

The chemical structure of polymers plays an important role in the static and dynamic behavior and in their corresponding practical applications. Poly-(methacrylate)s and poly-(acrylate)s are families of polymers which have been widely studied from different points of view, being their versatility well documented.<sup>1-3</sup> In some cases, small structural changes in the side chain, result in significant changes in their properties and hence in their potential applications.<sup>4-8</sup> For example, this type of polymers achieve high lithographic sensitivity combined with dry-etch durability in electron-beam resists depending on the added functional groups.<sup>9</sup> As another example, poly-(methacrylate)s and poly-(acrylate)s with aromatic groups in their side chains are used in combination with other monomers as materials in the area of ophthalmic devices. For this type of application, the polymer material must present a glass transition temperature not greater than about 37 °C, which is normal human body temperature, and also, an adequate flexibility. Polymers having glass transition temperatures higher than 37 °C would only be flexible at temperatures above 37 °C. So, for a convenient manipulation of the glaucoma filtration devices at room temperature, it is preferred to use polymers having a glass transition temperature somewhat below normal body temperature and no greater than room temperature, e.g., about 20-25 °C.<sup>10-</sup>

In order to obtain a better understanding of the chemical structure effect on the dynamics of the chains, it is important to carry out parallel studies with polymers exhibiting small differences in their structures. This type of analysis is interesting because the improvement of the properties of a polymeric material requires a better understanding of its molecular dynamics. For example, relaxation processes are determinant in the mechanical and electrical properties of polymers in engineering applications. Even in more sophisticated applications, chains dynamics have great importance. For example, the dipoles of chromophores groups anchored to a rigid backbone can be oriented by an electric field to accomplish anisotropy such that the material can be used in nonlinear optics purposes.<sup>12</sup>

The intensity of interactions between atoms, ions, or molecules determines the physical structure of the condensed matter. The glass transition temperature ( $T_g$ ) is a major phenomenon in condensed matter physics, the precursor of which is the so-called  $\alpha$ -relaxation. A general feature of polymer chains is the role played by intramolecular interactions in the development of the glass transition. For a homologous series of polymers, molecular flexibility and glass transition are straightforwardly related in such a way that the higher the flexibility, the lower the  $T_g$ . Moreover, the increase of intermolecular interactions, i.e. chain polarity, also produces an increasing of the glass transition temperature. A true understanding of the glass transition requires the solution of a several body problem caused by inter/intra-molecular interactions.

Dielectric relaxation spectroscopy has been used as an effective tool in order to obtain information about the dynamic behavior of polymers.<sup>13-15</sup> Consequently, the dielectric analysis of poly-(phenyl-propyl-acrylate) (P3Ph1PA) and poly-(phenyl-propyl-methacrylate) (P3Ph1PM) samples was carried out over a wide

frequency/temperature range, in order to gain a better understanding of the influence of the chemical structure on the dynamic behavior.

The aim of this paper is to study the effect of the methyl groups attached to the backbone of P3Ph1PM on the dynamic mobility when comparing to the P3Ph1PA. A scheme of the repeating units of P3Ph1PA and P3Ph1PM is shown in Figure 1.

## EXPERIMENTAL

### Sample preparation

Monomers were obtained by reaction of methacryloyl chloride with the corresponding alcohols in the presence of triethylamine as acid acceptor. Monomers were purified by distillation under reduced pressure. Polymerization was achieved in toluene, using AIBN as initiator, under vacuum during 48 h at 60 °C. Polymers were precipitated in methanol and vacuum dried. Monomers and polymers were characterized by FTIR and <sup>1</sup>H-NMR and the obtained results agree with the expected chemical structures.

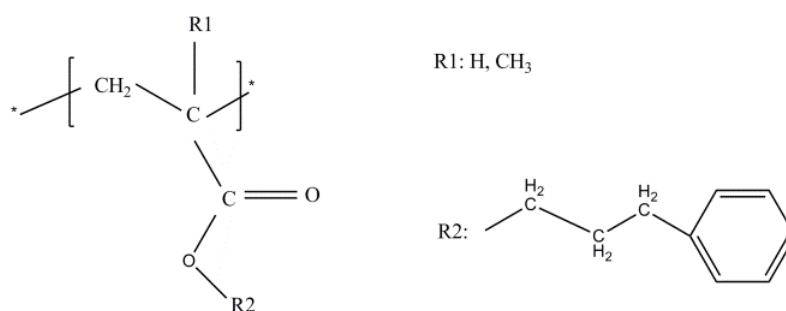


**Figure 1.** Scheme of chemical structure of P3Ph1PA (R<sub>1</sub>: H) and P3Ph1PM (R<sub>1</sub>: CH<sub>3</sub>) samples.

### **Differential Scanning Calorimetry Measurements (DSC)**

DSC measurements of P3Ph1PA and P3Ph1PM samples were carried out using a TA Instruments DSC Q-20 with a refrigerated cooling system. The thin films were repeatedly stacked into a pan, with a weight of 7.0 mg. The measurements were conducted in crimped non-hermetic aluminum pans, using an empty pan as reference. The DSC tests were performed under a 50 ml min<sup>-1</sup> flow of nitrogen to prevent oxidation. High-purity indium was used to calibrate the DSC cell. A first run was carried out in both samples in order to remove all the residual moisture and to erase the effect of previous thermal history. Thermograms were obtained in a second heating ramp from -80 to 120 °C for the P3Ph1PA and from -20 to 100 °C for the P3Ph1PM, at a heating rate of 20 °C min<sup>-1</sup>. The glass transition temperatures were evaluated as the intersection of the base line of the glassy region with the tangent to the endotherm in the middle points.

### **Dielectric Relaxation Spectroscopy (DRS)**

Isothermal relaxation spectra of P3Ph1PA and P3Ph1PM samples were collected by using a Novocontrol Broadband Dielectric Spectrometer (Hundsagen, Germany) consisting of an Alpha analyzer to carry out measurements from  $5 \times 10^{-2}$  to  $3 \times 10^6$  Hz. The measurements were carried out in inert N<sub>2</sub> atmosphere between -80 to 120 °C (P3Ph1PM) and -80 to 100 °C (P3Ph1PA), with a step of 5 °C. For the P3Ph1PA sample, an additional measurement between -15 and 30 °C with a step of 2 °C was carried out in order to get a better definition of the glass rubber transition zone. The temperature was controlled by a nitrogen jet (QUATRO from Novocontrol) with a temperature error of 0.1 °C during every single sweep in frequency. Molded disc shaped

samples of about 0.1  $\mu\text{m}$  thickness and 20 mm diameter was used. The experimental uncertainty was better than 5% in all cases.

## RESULTS AND DISCUSSION

### DSC Measurements

Figure 2 shows the DSC thermograms obtained for both polymers. The measured characteristic temperatures and heat capacity changes are summarized in Table 1.

The DSC thermogram corresponding to P3Ph1PA exhibits a single  $T_g$  at  $-12.7\text{ }^\circ\text{C}$  while the thermogram of P3Ph1PM presents two  $T_g$ s at  $10.1$  and  $32.6\text{ }^\circ\text{C}$ . In the inset of Figure 2 (b) are represented the derivate of heat flow, in order to a better determination of the two overlapped  $T_g$ s present in P3Ph1PM. As usual, the polymethacrylate displays a higher  $T_g$  than the corresponding polyacrylate.<sup>16,17</sup> The existence of two  $T_g$ s has been also observed in some poly(n-alkyl methacrylate)s with long side chains.<sup>18</sup> The physical interpretation of this behavior is related to the presence of different domains in which the dynamics are dominated either by the alkyl side chain or by the main chain. In some cases, the glass transition associated with these aggregates is not visible by DSC, but the existence of the domains can be revealed by means other experimental techniques as X-ray diffraction and neutron scattering. The obtained results using these techniques suggest that the side groups of different monomeric units tend to aggregate forming self-assembled alkyl nanodomains [called (PE)-like nanodomains].<sup>19-22</sup> Recently, we have found evidence of the existence of nanodomain aggregates in poly(dimethoxybenzyl methacrylate)s<sup>23</sup> and in poly-(2-ethoxyethyl methacrylate).<sup>24</sup>

However in both cases, the  $T_g$  associated with these aggregates was not observed by DSC.

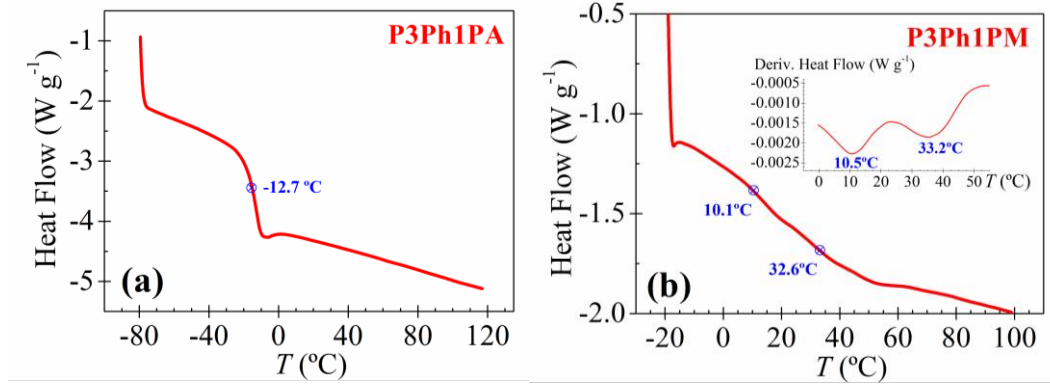


**Figure 2.** DSC experimental curves for (a) P3Ph1PA and (b) P3Ph1PM samples. Inset: Derivative representation of the heat flow.

**Table 1.** Characteristic Temperatures and Heat Capacity Changes of the P3Ph1PA and P3Ph1PM samples.

sample	P3Ph1PA	P3Ph1PM	
$T_{on}$ (°C)	-18.3	8.1	32.3
$T_{end}$ (°C)	-10.8	16.9	40.1
$\Delta T_g$ (°C)	-7.5	-8.8	-7.8
$T_g$ (°C)	-12.7	10.1	32.6
$\Delta C_p$ (J g <sup>-1</sup> K <sup>-1</sup> )	0.4391	0.1252	0.1013

In our case, the existence of the domains was identified by means of DSC, given the existence of two  $T_g$ s in the P3Ph1PM sample.

The temperature range of the glass transition ( $\Delta T_g = T_{end} - T_{on}$ ), which is a measure of the sample heterogeneity, is slightly higher for the P3Ph1PM when comparing with the P3Ph1PA, as expected. Moreover, the P3Ph1PA sample has a

higher heat capacity jump value ( $\Delta C_p$ ) at  $T_g$  than the P3Ph1PM ones. This parameter is related to the polymer fraction participating in the glass transition. Thus, the lower values of  $\Delta C_p$  obtained for the two transitions of P3Ph1PM are related to (i) the small proportion and size of the existing aggregates and (ii) the motion restriction imposed by the aggregates themselves.

### **DRS measurements**

The complex dielectric permittivity of P3Ph1PA and P3Ph1PM samples is plotted in Figure 3 as a function of temperature at five characteristic frequencies. The dielectric permittivity of P3Ph1PA sample presents one step associated with the glass rubber or  $\alpha$ -relaxation. On the other hand, two steps are observed for the P3Ph1PM associated with the two glass rubber transitions, which were also detected by DSC. In both samples, the  $\alpha$ -relaxation is followed by an increase of the permittivity related to the conductive interfacial processes. The loss factor isochrones show a well-developed  $\alpha$ -relaxation for the P3Ph1PA sample, whereas two overlapped  $\alpha$  processes are observed in the P3Ph1PM case. As usual, at high temperatures and low frequencies the  $\alpha$ -relaxation is masked by conductive contributions.

A more complete description of the relaxation behavior of the polymers is shown in Figure 4, where the complex dielectric permittivity in the frequency domain is presented at several temperatures. Again, the loss factor isotherms for the P3Ph1PA exhibit one  $\alpha$ -relaxation and strong conductive processes whereas two overlapped  $\alpha$ -relaxations are observed for the P3Ph1PM. Additionally, the low frequency  $\alpha$ -relaxation of the P3Ph1PM sample overlaps with an Maxwell-Wagner-Sillars (MWS) process.<sup>25-27</sup> The MWS absorption is associated with the build-up of charges at the interfaces

generated by the existence of side-chains nanodomains and appears as a shoulder in the dielectric spectra at frequencies lower than those of the  $\alpha$ -relaxations.

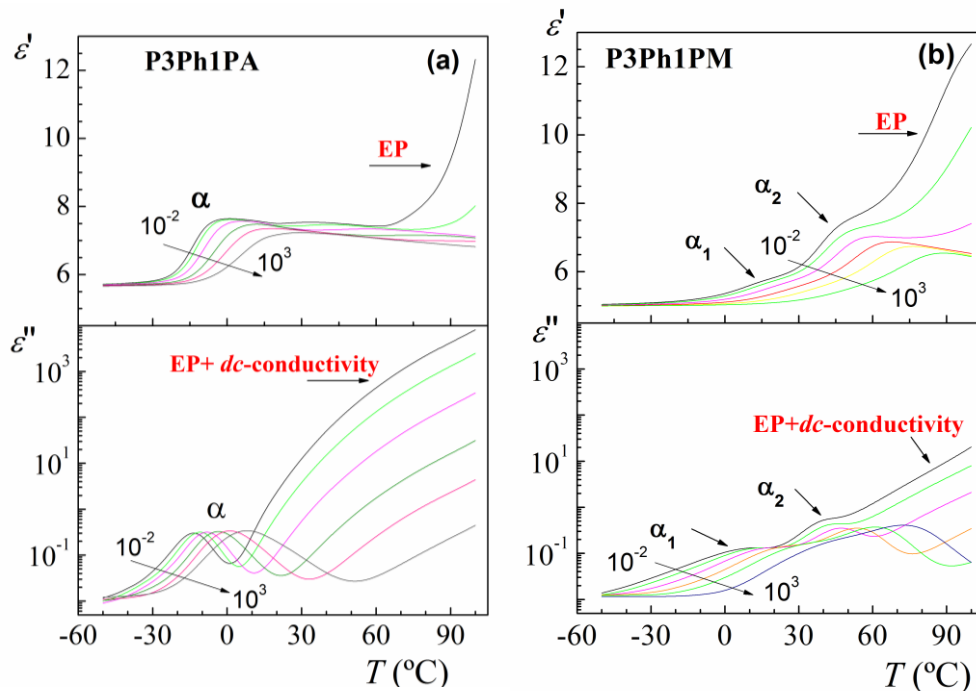


**Figure 3.** Temperature dependence of dielectric permittivity and loss factor at  $10^x$  Hz ( $x=-2, -1, 0, 1, 2$  and  $3$ ) for (a) P3Ph1PA and (b) P3Ph1PM.

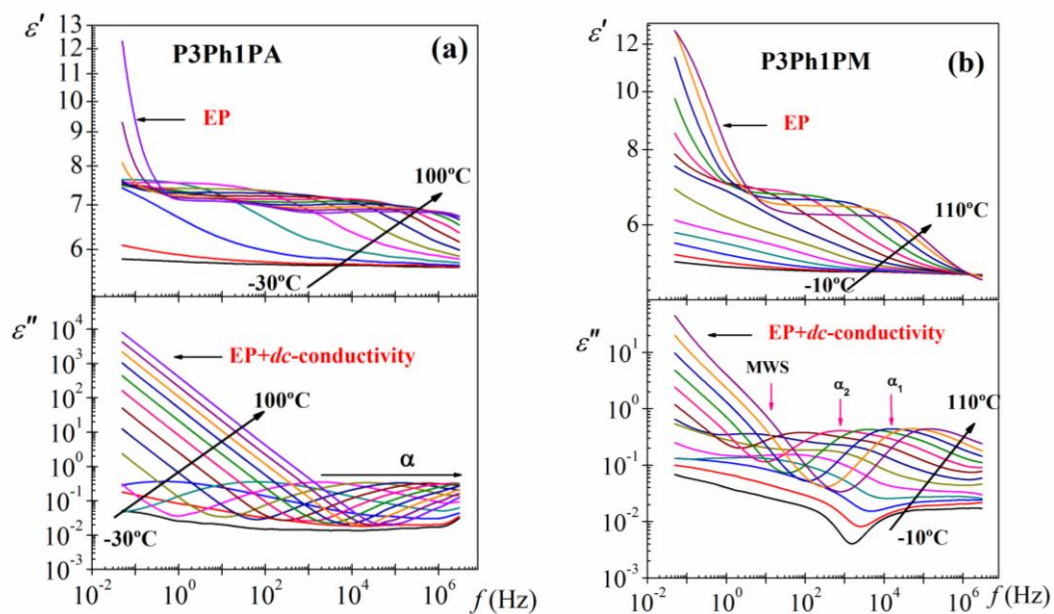


**Figure 4.** Dielectric permittivity and loss factor as a function of the frequency for (a) P3Ph1PA (from -30 to 100 °C, with a 10 °C step) and (b) P3Ph1PM (from -10 to 110 °C, with a 10 °C step).

Better definitions of the loss peaks are obtained by plotting the dielectric results in terms of the dielectric loss modulus,  $M''$ . Figure 5 (a) shows the isotherms of  $M''$  for the P3Ph1PA sample. It is observed two ostensible peaks corresponding in decreasing order of frequency to the  $\alpha$  and conductive processes. However, the isotherms of  $M''$  for the P3Ph1PM, shown in Figure 5 (b), exhibit two ostensible overlapped peaks corresponding to the  $\alpha_1$  and  $\alpha_2$ -relaxations and a wide and complex process at lower frequencies, associated with the conductive processes. So, the relatively narrow and symmetric conductive peak observed in the P3Ph1PA widens in the case of the P3Ph1PM as a result of the overlapping of the MWS process and the conductivity processes.

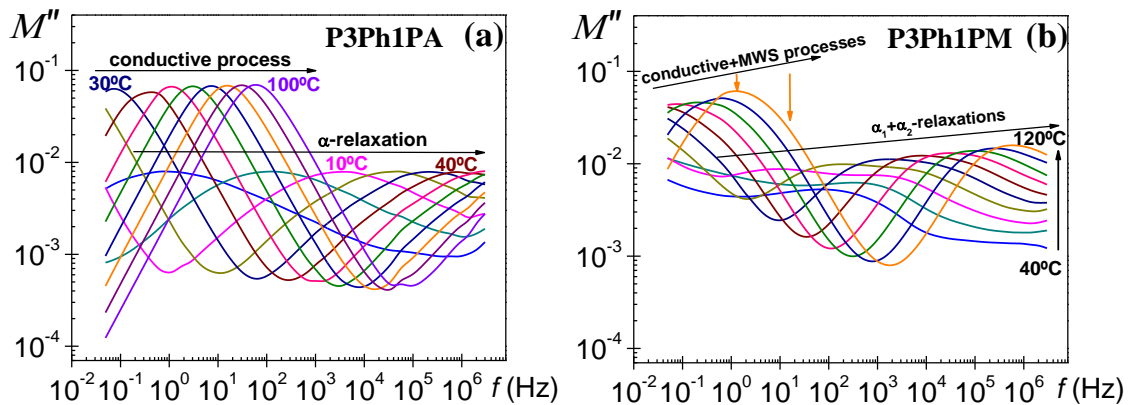


**Figure 5.** Dielectric loss modulus as a function of the frequency for (a) P3Ph1PA (from 10 °C to 100 °C, with a step of 10 °C) and (b) P3Ph1PM (from 40 °C to 120 °C, with a step of 10 °C).

In order to characterize the dielectric spectra of the structural isomers, the empirical Havriliak-Negami model (HN)<sup>28,29</sup> has been used

$$\varepsilon_{dip}^*(\omega) = \varepsilon_{\infty} + \frac{\varepsilon_0 - \varepsilon_{\infty}}{\left[1 + (j\omega\tau_{HN})^a\right]^b} \quad (1)$$

where the subscripts  $\varepsilon_0$  and  $\varepsilon_{\infty}$  are, respectively, the relaxed ( $\omega = 0$ ) and unrelaxed ( $\omega = \infty$ ) dielectric permittivities,  $\Delta\varepsilon$  is the strength relaxation,  $\tau_{HN}$  is the characteristic relaxation time associated with the relaxation and  $a$  and  $b$  are the shape parameters. These parameters are related, respectively, to the departure of the complex  $\varepsilon''$  vs  $\varepsilon'$  plot from a semi-circumference, at low frequencies, and to the skewness of the plot along a straight line, at high frequencies.<sup>30</sup> The  $a$  and  $b$  parameters fulfill the condition  $0 < a, b \leq 1$ , and for a Debye process  $a = b = 1$ .

For the P3Ph1PM sample, the characterization of the two  $\alpha$ -relaxations was carried out using an additive rule for the analysis of the dielectric loss spectra,<sup>31</sup>

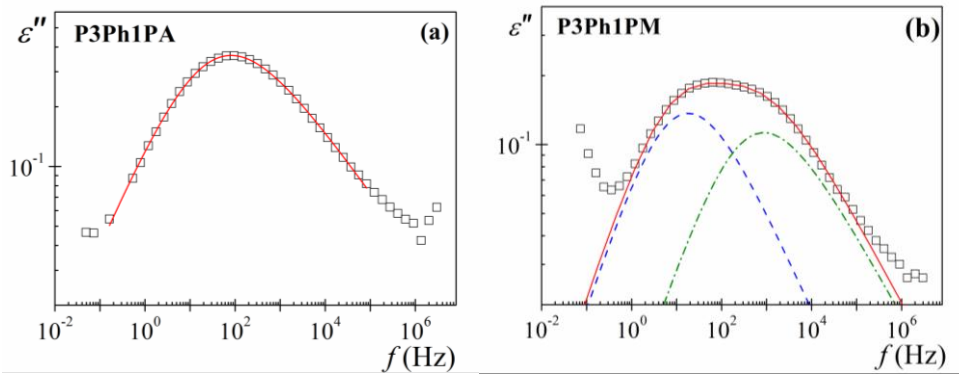
$$\varepsilon_{dip}'' = \text{imag} \left[ \sum_{i=1}^{i=2} \left( \Delta\varepsilon_i / \left[ 1 + (j\omega\tau_i)^{a_i} \right]^{b_i} \right) \right]$$

where the subscript  $i$  refers to the  $\alpha_1$  and  $\alpha_2$

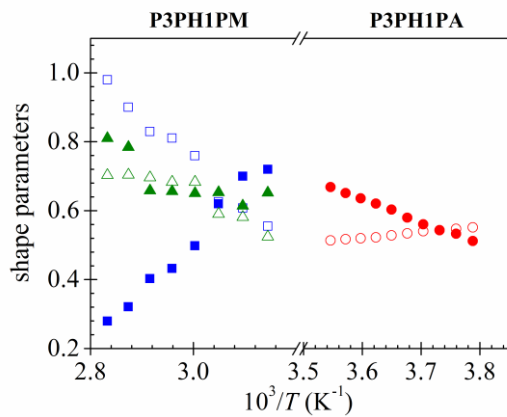
absorptions. As an example, in Figure 6 is depicted the fitting procedure for both samples at one temperature. The fit parameters determined at several temperatures from a multiple nonlinear regression analysis of the experimental data are summarized in Figures 7 to 9.

In the case of the P3Ph1PA the HN analysis was carried out each 2 °C, in order to get a better characterization of the dielectric spectrum in the glass rubber transition zone, and to verify that it was a single process. Values of the shape parameters for both polymer samples are shown in Figure 7. For the P3Ph1PA the  $a$ -parameter slightly decreases with increasing temperature, unlike the  $b$ -parameter, which significantly

increases with the temperature. A rather different scenario is found for the shape parameters of the  $\alpha$ -relaxation processes of P3Ph1PM. In this case, the  $a$ -parameter values increase with temperature. The relatively high values of  $a$ -parameter obtained at high temperatures for one of the  $\alpha$ -relaxations suggests that the complexity of this process decreases with increasing temperature. On the other hand, the value of the  $b$ -parameter increases with the temperature for one of the relaxations while decreases for the other.

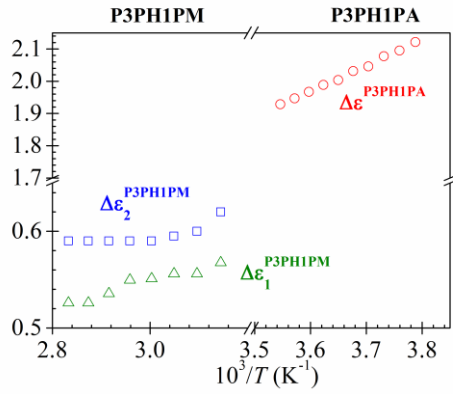


**Figure 6.** Deconvolution of loss factor for (a) P3Ph1PA (at 1 °C) and (b) P3Ph1PM (at 50 °C) Squares represent the experimental data, continuous line the HN fitting curve, and dashed lines the individual processes.



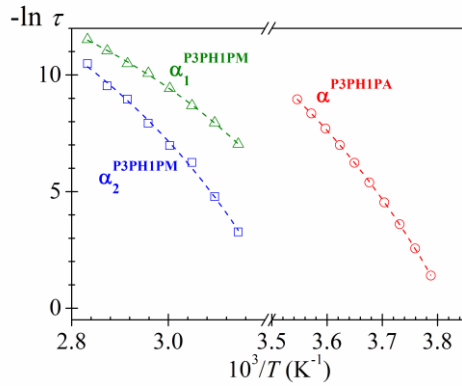
**Figure 7.** Temperature dependence of the  $a$  (open symbol) and  $b$  (filled symbols) shape parameters of the  $\alpha$ -processes for P3Ph1PA (circle) and P3Ph1PM (square [ $\alpha_1$ ] and triangle [ $\alpha_2$ ]) samples.

Figure 8 shows the temperature dependence of the relaxation strength for the processes of P3Ph1PA and P3Ph1PM samples. Values of all  $\alpha$ -processes ( $\Delta\varepsilon_\alpha$ ) follow the classical trends, that is, the strength decreases with increasing temperature. This behavior is due to the fact that thermal energy disturbs the alignment of the molecule dipoles intervening in the cooperative motions that give rise to the relaxation. Moreover, the  $\Delta\varepsilon_\alpha$  values for the P3Ph1PA are significantly higher than those of the P3Ph1PM. The strength of the segmental relaxation is not only related to the polymer fraction participating in the glass rubber transition but also to the dipolar moment of the polymer units. In our case, the difference in the dipolar moment of both polymer units is not enough to justify the observed variation in the  $\Delta\varepsilon_\alpha$  values. Thus, the increase in the  $\Delta\varepsilon_\alpha$  values for the P3Ph1PA sample is probably due to a higher polymer fraction participating in the glass transition process. Taking into account that  $\Delta C_p$  DSC parameter is also an indicative of the polymer fraction involved in the  $T_g$ , the obtained results from both techniques, are in good agreement, since  $\Delta C_p$  was found higher for the P3Ph1PA than for the P3Ph1PM.



**Figure 8.** Temperature dependence of the strengths of the  $\alpha$ -processes for P3Ph1PA (open circle) and P3Ph1PM (open square [ $\alpha_1$ ] and triangle [ $\alpha_2$ ]) samples.

Figure 9 shows the temperature dependence of the relaxation times associated with the maximum of the peak of the  $\alpha$  processes of both samples.<sup>32</sup>



**Figure 9.** Arrhenius plot for the  $\alpha$ -processes for P3Ph1PA (open circle) and P3Ph1PM (open square and triangle) samples. Dashed lines correspond to VFTH fitting curves.

As usual, the  $\alpha$ -relaxation is described by the Vogel-Fulcher-Tammann-Hesse (VFTH) equation<sup>33-35</sup> expressed in terms of the strength coefficient  $D_0$ <sup>36-38</sup> by

$$\tau = \tau_0 \cdot \exp\left(\frac{D_0 \cdot T_v}{T - T_v}\right) \quad (2)$$

where  $\tau_0$  is a pre-factor and  $T_V$  is the Vogel temperature currently associated with the temperature at which the entropies of the glassy system and the crystal are similar, i.e. the configurational entropy of the glassy system is null. Generally, the  $T_V$  value is about 50 K below the  $T_g$  of the polymers. Values of the parameters that fit Eqn (2) to the experimental results are collected in Table 2. The results show that  $D_0$  parameter is in all cases lower than 10, the limit value which separates fragile materials ( $D_0 < 10$ ) from strong ones ( $D_0 > 10$ ).<sup>35,38</sup> By comparing Eqn (2) with the Doolittle equation,<sup>39,40</sup> the relative free volume at  $T_g$  ( $\phi_g/B = (T_g - T_V)/D_0 \cdot T_V$ ) and the thermal expansion coefficient ( $\alpha_f = 1/D_0 \cdot T_V$ ) were evaluated (see Table 2). The obtained values for the relative free volume are slightly higher than the reported average value, but similar to other poly(methacrylates) with phenyl groups in the side chain, previously reported by us.<sup>23</sup> On the other hand, the values of thermal expansion coefficient are in agreement with those reported for other flexible polymers,<sup>41</sup> which lie in the vicinity of  $5 \times 10^{-4} \text{ K}^{-1}$ .

**Table 2.** Characteristic parameters of the dipolar and conductivity processes of the P3Ph1PA and P3Ph1PM samples.

sample	P3Ph1PA	P3Ph1PM	
$\log_{10} \tau_0[\text{s}]$	-11.8±0.2	-9.6±0.1	-8.9±1.5
$D_0$	5.0±0.3	5.2±0.7	4.2±0.8
$T_V$ (K)	222.5±1.1	236.3±5.4	257.2±1.8
$\phi_g/B \cdot 10^2$	3.4±0.2	3.8±0.5	4.5±0.5
$\alpha_f \times 10^4$ (K <sup>-1</sup> )	8.9±0.4	8.2±0.9	9.3±1.1
$m$	80.5±5.0	68.8±5.0	61.3±5.0
$m^*$	81.9	88.3	94.5
$E_a(T_g)$ (kJ mol <sup>-1</sup> )	442±19	373±16	359±30
$E_a^*(T_g)$ , kJ·mol <sup>-1</sup>	371	446	524

In order to rationalize the departure of supercooled liquids from Arrhenius behavior in the vicinity of the glass transition temperature, Angell introduced in the 1980s the concept of dynamic fragility.<sup>42</sup> The dynamic fragility index,  $m$ , characterizes how rapidly the properties of the system vary as the temperature of a supercooled liquid approaches its glass transition, and is defined as<sup>43</sup>

$$m = \lim_{T \rightarrow T_g} \left[ \frac{d \log \tau}{d(T_g/T)} \right] \quad (3)$$

Obviously, as  $m$  decreases, the temperature dependence of the relaxation time comes closer to the Arrhenius behavior. Taking  $\tau_g$  as reference and considering that the temperature dependence of the  $\alpha$ -relaxation, for flexible polymers and liquids, is governed by Eqn (2), the fragility parameter can be written as

$$m = \frac{D_0 \cdot T_v}{2.303 T_g \cdot (1 - T_v/T_g)^2} \quad (4)$$

The values of  $m$  for both samples (Table 2), show that the dynamic fragility index for the P3Ph1PA is higher than those obtained for the P3Ph1PM. This trend is in agreement with the Angell's energy landscape model, which predicts that larger  $\Delta C_p$  ( $T_g$ ) values are associated with a more fragile behavior.<sup>36,44</sup>

Qin and McKenna<sup>45</sup> compiled literature data for dynamic fragility of different types of glass-forming liquids, showing a roughly linear increase in  $m$  with increasing  $T_g$ . The pertinent expressions were  $m^* = 0.28(\pm 0.067) \cdot T_g(\text{K}) + 9(\pm 20)$  for polymers and  $m^* = 0.25(\pm 0.059) \cdot T_g(\text{K}) + 16(\pm 10)$  for hydrogen bonding organics and organic and inorganic ionic glasses. The values of  $m^*$  calculated by the former expression for P3PH1PA and P3PH1PM, are collected in Table 2. The  $m^*$  value for P3Ph1PA is in

rather good agreement with the one obtained by using Eqn (4). However, the experimental results for the P3Ph1PM are nearly 30% below of those predicted by the straight line proposed by Qin and McKenna. Similar discrepancy between both values has been previously observed in other systems where the nanodomains existence was verified.<sup>23</sup>

As showed in Figure 4, the MWS process is only clearly observed in the P3Ph1PM sample. This process appears to be hindered at high and low frequency zones by the  $\alpha$  and the conductive processes, respectively. For this reason it was unfeasible its characterization. Perhaps, this process is also present in P3Ph1PA spectrum, but with a much lower intensity than in the case of P3Ph1PM.

In order to analyze the conductive process that dominates the dielectric spectra at high temperatures and low frequencies, the *ac* conductivity has been calculated from the dielectric permittivity according to the relation:  $\sigma^*(\omega) = j \cdot \omega \cdot e_0 \cdot \varepsilon^*(\omega)$  being  $e_0$  the vacuum permittivity. In general, at a constant temperature the *ac* conductivity can be expressed as<sup>46</sup>

$$\sigma'(\omega) = \sigma_{dc} + A\omega^s \quad (5)$$

where  $\sigma_{dc}$  is the frequency-independent conductivity ( $\omega \rightarrow 0$ ),  $A$  is a temperature dependent factor and  $s$  is the frequency exponent ( $0 \leq s \leq 1$ ) also depending on the temperature.

Figure 10 (a) and (b) depicts the dependence of the *ac* conductivity with the frequency of the applied field at several temperatures for both samples. In the low frequency and high temperature zone, a frequency independent conductivity is recorded, which is attributed to resistive conduction through the bulk of polymer. On the other hand, when frequency is raised, the main displacement of the charge carriers is reduced.

At this point the real part of the conductivity, after reaching a certain frequency,  $\omega_c$ , becomes proportional to frequency following the law  $\sigma'_{ac}(\omega) \sim \omega^s$  with  $0 \leq s \leq 1$ . However, the influence of temperature is more pronounced in the low frequency range, while at high frequencies, the ac conductivity curves collapse.

In Figure 10 (c) are plotted the values of *dc* conductivity obtained at several temperatures from extrapolations to low frequencies as a function of the reciprocal temperature for both samples. As it can be seen, in the case of the P3Ph1PA a curvature according to a VFTH description was observed. On the contrary, the P3Ph1PM sample showed the opposite curvature. This anomalous behavior is most likely due to the interference of the MWS relaxation in the determination of the 'pure' d.c. conductivity.

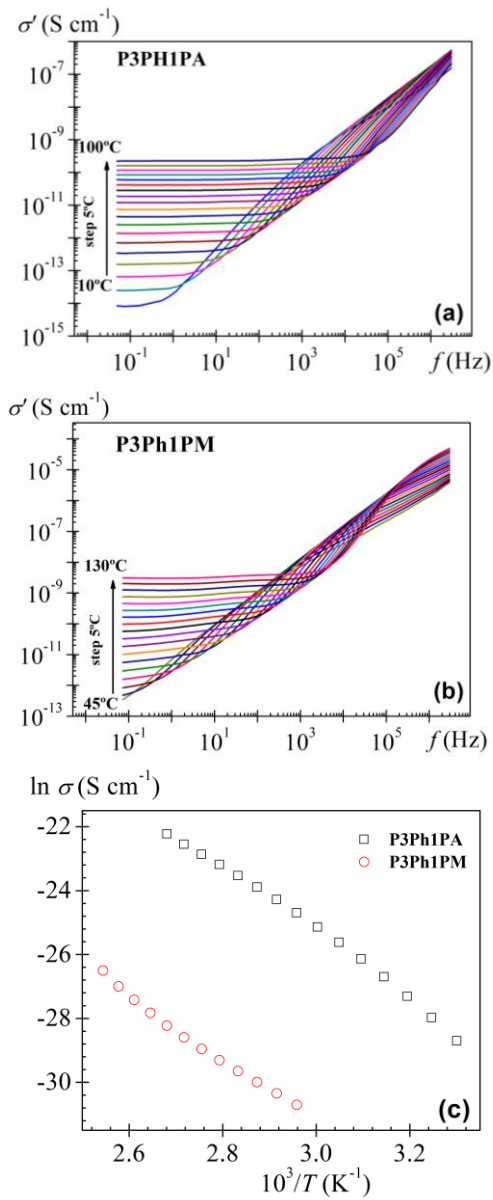


**Figure 10.** Frequency dependence of the *ac* conductivity, at several temperatures, of (a) P3Ph1PA, (b) P3Ph1PM. (c) Temperature dependence of *dc* conductivity for both samples.

## CONCLUSIONS

According to our analysis, slight differences in the chemical structure, as the presence of a methyl group instead of a hydrogen atom, produce significant changes in

the dynamic mobility of the polymer samples under study. Thus, the presence of the methyl group in the P3Ph1PM promotes the nanophase separation of the incompatible main and side chains and consequently, the generation of nanodomains. All the employed techniques were in agree and showed the existence of the nanodomains in the P3Ph1PM sample:

- (i) From the DSC thermogram, the existence of the nanodomains is evidenced by the presence of two  $T_g$ s, associated with the main and side chain parts.
- (ii) From the DRS spectra the nanodomains are also proved by the observation of two  $\alpha$ -relaxations and by the presence of the MWS process, the latter associated with the build-up of charges at the interfaces of the side-chains nanodomains.
- (iii) Moreover, higher values of  $\Delta C_p$  and  $\Delta \varepsilon_\alpha$  parameters were observed for the P3Ph1PA when comparing to the P3Ph1PM. Both parameters are associated with a higher fraction of polymer contributing to the glass rubber transition, pointing out that the methyl group disturbs the molecular mobility and promotes the nanodomains formation.
- (iv) As usual, for both polymers, the  $\alpha$ -relaxation is described by the VFTH equation. The relative free volumes obtained are slightly higher than the average values reported in the literature, but similar to other poly(methacrylates) with phenyl groups in the side chain.

## **ACKNOWLEDGEMENTS**

B.R.F, P.O.S, M.C, and M.J.S., gratefully acknowledge to CICYT for grant MAT2012-33483. D.R. and A.L. acknowledge to Fondecyt grant 1120091.

## REFERENCES

1. McCrum NG, Read BE, Williams W, *In Anelastic and Dielectric Effects in Polymeric Solids*; Dover Publications: New York (1991).
2. Heijboer J, *Molecular basis of transitions and relaxation*. In: Meier DJ, editor. Midland macromolecular monographs, vol. 4; London: Gordon&Breach (1978).
3. Heijboer J, PhD Thesis. Leiden, The Netherlands (1972).
4. Kine BB, Novak RW, *Acrylic and Methacrylic Ester Polymers in Encyclopedia of Polymer Science and Engineering*; Wiley: New York (1985), 262.
5. Stickler M, Rhein T, *Polymethacrylates in Ullmann's Encyclopedia of Industrial Chemistry*; 5th ed., Elvers, B.; Hawkins, S.; Schultz, G. Eds. VHS: New York (1992), A21.
6. Hawkins S, Schultz G, Eds. VHS: New York, (1992), A21, 473.
7. Gaborieau M, Graf R, Kahle S, Pakula T, Spiess HW, *Macromolecules* **40**:6249-6256 (2007).
8. Huang GS, Jiang LX, Li Q, *J. Appl. Polym Sci.* **85**:746-751 (2002).
9. Jones RG, Harry Cragg R, Davies RDP, Brambley DR, *J. Mater. Chem.* **2(4)**:371-377 (1992).
10. Laredo WR, *UV/visible light absorbers for ophthalmic lens materials*, US8262947 B2, 6 January (2011).
11. Graff G, Karakelle M, Sheets JW, Yanni JM, *Materials for use in glaucoma filtration devices*, EP0914169 A2, 22 May (1999).
12. Riande E, Saiz E, *Dipole Moments and Birefringence of Polymers*; Prentice-Hall, Englewood Cliffs, NJ, (1992).

13. Williams G, *Dielectric Relaxation Spectroscopy of Amorphous Polymer Systems in Keynote Lectures in Polymer Science*, edited by E. Riande CSIC, Madrid, (1995).
14. Kremer F, Schönhals A, *In Broadband Dielectric Spectroscopy*, Springer: Berlin, (2003).
15. Riande E, Díaz-Calleja R, *In Electrical Properties of Polymers*; Dekker, M., Ed.; The United States of America, (2004).
16. Fleischhaker F, Haehnel AP, Misske AM, Blanchot M, Haremza S, Barner-Kowollik C, *Macromolecular Chemistry and Physics* **215(12)**:1192–1200 (2014).
17. Saez-Torres P, Sanchis MJ, Diaz-Calleja R, Guzman J, Riande E, *Journal of Applied Physics* **88(3)**:1593-1599 (2000).
18. Strella S, Chinai SN, *Journal Polymer Science* **31(122)**:45-52 (1958).
19. Beiner M, Kahle S, Abens S, Hempel E, Höring S, Meissner M, Donth E, *Macromolecules* **34**:5927-5935 (2001).
20. Beiner M, *Macromol. Rapid Commun.* **22**:869-895 (2001).
21. Beiner M, Huth H, *Nature Mater.* **2**:595-599 (2003).
22. Arbe A, Genix AC, Arrese-Igor S, Colmenero J, Richter D, *Macromolecules* **43**:3107–3119 (2010).
23. Sanchis MJ, Carsí M, Ortiz-Serna P, Domínguez-Espinosa G, Díaz-Calleja R, Riande E, Alegría L, Gargallo L, Radic' D, *Macromolecules* **43**:5723–5733 (2010).
24. Carsí M, Sanchis MJ, Díaz-Calleja R, Riande E, Nugent MJD, *Macromolecules* **45**:3571-3580 (2012).
25. Maxwell JC, *Electricity and Magnetism*; Clarendon: Oxford (1893).
26. Wagner KW, *Arch. Elektrotech.* **2**:371-387 (1914).
27. Sillars RW, *Inst. Electr. Eng.* **80**:378-394 (1937).

28. Havriliak S, Negami S, *Polymer* **8(4)**: 161-210 (1967).
29. Havriliak S, Negami S, *J. Polym. Sci. Polym. Symp.* **14**:99-117 (1966).
30. Havriliak S, Havriliak SJ, *Dielectric and Mechanical Relaxation in Materials*; Hanser: Munich (1997), p 57.
31. Donth E, *J. Polym. Sci. Part B Polym. Phys.* **34(17)**:2881–2892 (1996).
32. Boersma A, van Turnhout J, Wübbenhorst M, *Macromolecules* **31**:7453-7460 (1998).
33. Vogel H, *Z Phys.* **22**:645-646 (1921).
34. Fulcher GS, *J Am Ceram Soc.* **8**:339-340 (1925).
35. Tamman G, Hesse W, *Z Anorg Allg Chem.* **156**:245-247 (1926).
36. Angell CA, *Science* **267**:1924-1935 (1995).
37. Angell CA, *In Complex Behavior of Glassy Systems*; Proceedings of the XIV Sitges Conference, Sitges, Barcelona, Spain. 10-14 June (1996).
38. Rubi M, Pérez-Vicente C, Eds. *In Complex Behavior of Glassy Systems*; Eds. Springer: Berlin (1997).
39. Doolittle AK, *J. Appl. Phys.* **22**:1471-1475 (1951).
40. Doolittle AK, *J. Appl. Phys.* **23**:236-239 (1952).
41. Ferry JD, *Viscoelastic Properties of polymers*; 2nd ed.; John Wiley & Sons: New York (1961).
42. Angell CA, *J. Non-Cryst. Solids* **73**:1-17 (1985).
43. Plazek DJ, Ngai KL, *Macromolecules* **24**:1222-1224 (1991).
44. Angell CA, *J. Non-Cryst. Solids* **131-133**:13-31(1991).
45. Qin Q, McKenna B, *J. Non-Cryst. Solids* **352**:2977-2985 (2006).

46. Jonscher AK, *Universal relaxation law*; Chelsea Dielectric Press: London (1992),  
Chapter 5.

## Figure Caption

**Figure 1.** Scheme of chemical structure of P3Ph1PA (R1: H) and P3Ph1PM (R1: CH<sub>3</sub>) samples.

**Figure 2.** DSC experimental curves for (a) P3Ph1PA and (b) P3Ph1PM samples. Inset: Derivative representation of the heat flow.

**Figure 3.** Temperature dependence of dielectric permittivity and loss factor at 10<sup>x</sup> Hz (x=-2, -1, 0, 1, 2 and 3) for (a) P3Ph1PA and (b) P3Ph1PM.

**Figure 4.** Dielectric permittivity and loss factor as a function of the frequency for (a) P3Ph1PA (from -30 to 100 °C, with a 10 °C step) and (b) P3Ph1PM (from -10 to 110 °C, with a 10 °C step).

**Figure 5.** Dielectric loss modulus as a function of the frequency for (a) P3Ph1PA (from 10 °C to 100 °C, with a step of 10 °C) and (b) P3Ph1PM (from 40 °C to 120 °C, with a step of 10 °C).

**Figure 6.** Deconvolution of loss factor for (a) P3Ph1PA (at 1 °C) and (b) P3Ph1PM (at 50 °C) Squares represent the experimental data, continuous line the HN fitting curve, and dashed lines the individual processes.

**Figure 7.** Temperature dependence of the *a* (open symbol) and *b* (filled symbols) shape parameters of the  $\alpha$ -processes for P3Ph1PA (circle) and P3Ph1PM (square [ $\alpha_1$ ] and triangle [ $\alpha_2$ ]) samples.

**Figure 8.** Temperature dependence of the strengths of the  $\alpha$ -processes for P3Ph1PA (open circle) and P3Ph1PM (open square [ $\alpha_1$ ] and triangle [ $\alpha_2$ ]) samples.

**Figure 9.** Arrhenius plot for the  $\alpha$ -processes for P3Ph1PA (open circle) and P3Ph1PM (open square and triangle) samples. Dashed lines correspond to VFTH fitting curves.

**Figure 10.** Frequency dependence of the ac conductivity, at several temperatures, of (a) P3Ph1PA, (b) P3Ph1PM. (c) Temperature dependence of *dc* conductivity for both samples.